

Phases of Pseudo-Nambu-Goldstone Bosons

Fotis Koutroulis,^a Matthew McCullough,^b Marco Merchand,^{a,c,d} Stefan Pokorski^a and Kazuki Sakurai^a

^a*Institute of Theoretical Physics, Faculty of Physics, University of Warsaw, ul. Pasteura 5, 02-093 Warsaw, Poland*

^b*CERN, Theoretical Physics Department, Geneva 23 CH-1211, Switzerland*

^c*KTH Royal Institute of Technology, Department of Physics, SE-10691 Stockholm, Sweden*

^d*The Oskar Klein Centre for Cosmoparticle Physics, AlbaNova University Centre, SE-10691 Stockholm, Sweden.*

E-mail: fotis.koutroulis@fuw.edu.pl, matthew.mccullough@cern.ch, marcomm@kth.se, stefan.pokorski@fuw.edu.pl, kazuki.sakurai@fuw.edu.pl

ABSTRACT: We study the vacuum dynamics of pseudo-Nambu-Goldstone bosons (pNGBs) for $SO(N+1) \rightarrow SO(N)$ spontaneous and explicit symmetry breaking. We determine the magnitude of explicit symmetry breaking consistent with an EFT description of the effective potential at zero and finite temperatures. We expose and clarify novel additional vacuum transitions that can arise for generic pNGBs below the initial scale of $SO(N+1) \rightarrow SO(N)$ spontaneous symmetry breaking, which may have phenomenological relevance. In this respect, two phenomenological scenarios are analyzed: thermal and supercooled dark sector pNGBs. In the thermal scenario the vacuum transition is first-order but very weak. For a supercooled dark sector we find that, depending on the sign of the explicit symmetry breaking, one can have a symmetry-restoring vacuum transition $SO(N-1) \rightarrow SO(N)$ which can be strongly first-order, with a detectable stochastic gravitational wave background signal.

Contents

1	Introduction	1
2	pNGB Potential Regime of Validity	3
3	Gegenbauer Goldstones	6
3.1	pNGB Potentials at Zero Temperature	7
3.2	pNGB Potentials at Finite Temperature	8
4	Cosmological Gegenbauer Phases	11
4.1	Hot Dark Sector	11
4.2	Supercooled Dark Sector	13
5	Summary and conclusions	19
A	Hot Sector Calculations	20

1 Introduction

PNGBs [1, 2] arise in nature, as phonons, magnons, pions and in a broad range of theoretical scenarios. It is no surprise that they are abundant. It is a theorem that whenever a continuous global symmetry is spontaneously broken that NGBs will arise [2]. Furthermore, it is widely believed that there can be no exact continuous global symmetries in nature (more precisely, in gravitational theories [3–7]), in which case any NGB will, in reality, be a pNGB. Thus, while the effective field theory (EFT) description of the low-energy behaviour of exact NGBs is an interesting object for theoretical study, it is likely that in nature the physics below the scale of spontaneous symmetry breaking is dominated by the scalar potential generated for pNGBs, since it contains the most relevant operators.

Since the structure of the pNGB potential determines the vacuum dynamics it is well-motivated to map the connections between explicit symmetry breaking sources in a UV theory and the vacuum structure and dynamics in the IR, since this aspect is physically relevant for pNGBs that are realised in nature. Once this map is firmly established one can then determine and/or classify the plausible phases of pNGB vacua and their dynamics.

Ref. [8] established the first part of this programme for an $SO(N+1) \rightarrow SO(N)$ spontaneous and explicit symmetry breaking pattern. The fundamental building blocks of explicit symmetry breaking were found to be the irrep spurions of $SO(N+1)$ which preserve an $SO(N)$ subgroup. Each such spurion gives rise, in the IR, to a unique Gegenbauer scalar potential which is an eigenfunction of the Laplacian on the N -sphere. Any general pNGB potential for $SO(N+1) \rightarrow SO(N)$ can thus be decomposed as a sum of Gegenbauer polynomials. Note that this is strongly analogous to the solution of the Hydrogen wavefunction

in quantum mechanics. The angular momentum $|j, 0\rangle$ eigenstates correspond to a non-zero expectation value for the spin- j irrep of $\text{SO}(3)$ which gives rise to the j^{th} Legendre polynomial, which is simply an $\text{SO}(3) \rightarrow \text{SO}(2)$ Gegenbauer polynomial. Any wavefunction which is a superposition of angular momentum eigenstates may be written as a sum of Legendre polynomials. Thus what we are familiar with for angular momentum in Hydrogen maps to the pNGBs of $\text{SO}(N+1) \rightarrow \text{SO}(N)$ breaking, where the spatial rotation global symmetry becomes an internal global symmetry.

With this organisation of pNGB potentials complete the next logical step, which is to understand the vacuum dynamics, is the focus of this work. Throughout we are concerned with the same $\text{SO}(N+1) \rightarrow \text{SO}(N)$ spontaneous and explicit symmetry breaking pattern. We focus for the most part, as a benchmark, on a single Gegenbauer pNGB potential, in the understanding that the lessons learned will map, in a straightforward way, into a sum of Gegenbauer potentials for any form of pNGB potential.

We begin by ascertaining the conditions under which the EFT description of the potential is valid, both at zero and finite temperature (specifically in the region of an interesting vacuum transition). This effectively places a quantitative constraint on the magnitude of the explicit symmetry breaking tolerable. Violation of this constraint implies a potential for which one does not have a controlled series expansion in the explicit symmetry breaking, whether at tree-level or at higher loop orders.

Subject to this constraint we then explore the vacuum dynamics for pNGBs, which we find to be rich and varied. It should be noted that throughout there is explicit $\text{SO}(N+1) \rightarrow \text{SO}(N)$ breaking thus, in terms of exact global symmetries, there is no formal phase transition, since only $\text{SO}(N)$ is an exact symmetry of the Lagrangian. However, since this explicit symmetry breaking is small, one does have a sense in which the fields, which play the role of order parameters, undergo vacuum transitions.

In this work we find that below the scale of spontaneous $\text{SO}(N+1) \rightarrow \text{SO}(N)$ breaking, which is driven by the development of a non-zero value for the $\text{SO}(N+1)$ radial mode, there are generically additional pNGB vacuum transitions. There is an additional critical temperature at which the pNGBs themselves develop a vacuum expectation value, triggering a further stage of spontaneous $\text{SO}(N) \rightarrow \text{SO}(N-1)$ breaking. This breaking is due to the explicit symmetry breaking, but the change in order parameter is independent of the magnitude of the explicit symmetry breaking. The reverse can also occur, with a pattern of $\text{SO}(N+1) \rightarrow \text{SO}(N-1)$ breaking followed by a further stage of $\text{SO}(N-1) \rightarrow \text{SO}(N)$ symmetry restoration at lower temperatures.

It follows to determine the nature of these pNGB vacuum transitions. There are two classes to consider, namely thermal and supercooled. In the thermal case we find that the transition is generically weakly first-order. On the other hand, when the pNGB sector is supercooled we find that the vacuum transition, leading to symmetry restoration, can be strong enough to generate detectable GW signatures. We finish with conclusions and future speculations.

2 pNGB Potential Regime of Validity

We consider an EFT containing the pNGBs ψ arising from the spontaneous breaking of an approximate global symmetry at the scale f . We define the action at zero temperature as

$$\mathcal{L} = \frac{1}{2}g_{ij}(\psi)\partial_\mu\psi^i\partial^\mu\psi^j + \mathcal{O}(\partial^4) - \varepsilon V_\varepsilon(\psi) - \varepsilon^2 V_{\varepsilon^2}(\psi) - \mathcal{O}(\varepsilon^3) + \dots + \mathcal{L}^{\text{CT}} \quad , \quad (2.1)$$

where we have Taylor expanded in derivatives and in ε , which is, by assumption for pNGBs, a small parameter associated with a source of explicit symmetry breaking. \mathcal{L}^{CT} represents the counterterms required for renormalisation.

Before commencing with any concrete calculations some considerations are in order concerning the validity of this EFT. To be effective, it must be valid for some range of energies and field scales. For the former, scattering amplitudes involving derivatives will scale as $(p^2/M^2)^j$, where j is some integer and M is the cutoff energy of the EFT, often associated with the mass of the radial mode of spontaneous symmetry breaking or some other UV scale such as the mass scale of intermediate vector resonances. In any case, the EFT description breaks down, by assumption, whenever $|p^2| \sim M^2$.

Equally important is the parameter ε . In order to be considered pNGBs there must be some range of field values over which there is some sensible notion of perturbative calculability within the EFT and of a scale separation with the UV. For pNGBs the field range is periodic in the spontaneous symmetry-breaking scale $\sim 2\pi f$. Due to this periodicity we will require that the EFT description is valid and affords a degree of perturbative calculability over all pNGB field values.

To determine the potential limits on the magnitude of ε it is helpful to consider the case of pions. Were the quark masses to be comparable to the QCD scale, or the QED gauge coupling to be $e \sim 4\pi$ in the vicinity of the QCD scale, there would be no sense in which one would have had light pions at all, as they would naturally have mass at the QCD scale. Following this, it is tempting to diagnose EFT validity using the pNGB masses. However, mass-scale separation alone seems insufficient. For instance, in a scenario with two large sources of explicit symmetry breaking $\varepsilon_1, \varepsilon_2 \sim 1$ one could in principle fine-tune their independent contributions to a pNGB potential to give a small mass-squared in the global vacuum, generating a scale separation $m_\psi^2 \ll M^2$. However, one would have no control over perturbative corrections to the form of the pNGB potential, either at tree-level at the matching scale or in the IR at higher loops, due to the underlying magnitude of explicit symmetry breaking. We must therefore be more pragmatic in determining the requirement on ε for the EFT description to be valid. The condition cannot simply be that $m_\psi^2 \ll M^2$, which is seemingly necessary but not sufficient. Therefore we opt for the imprecise, but practical, condition that the pNGB potential at $\mathcal{O}(\varepsilon)$ must be a good approximation to the full potential with all quantum corrections included. In other words, while $\mathcal{O}(\varepsilon^2)$ and higher terms will exist, they must not qualitatively alter the form of the pNGB potential.

The one-loop Coleman-Weinberg potential provides a useful diagnostic in this respect. For pNGBs this is given by [8–10]

$$V^{\text{CW}} = \frac{1}{2}\text{Tr} \int \frac{d^4p}{(2\pi)^4} \log \left[p^2 + \varepsilon g^{-1} \left(\frac{\delta^2 V_\varepsilon}{\delta\psi^2} - \frac{\delta V_\varepsilon}{\delta\psi} \Gamma \right) \right] \quad , \quad (2.2)$$

where Γ are the Christoffel symbols. The field-dependent curvature (or mass-squared) entering this expression is

$$\mathcal{M}_\varepsilon^2(\psi) = \varepsilon g^{-1} \left(\frac{\delta^2 V_\varepsilon}{\delta \psi^2} - \frac{\delta V_\varepsilon}{\delta \psi} \Gamma \right) , \quad (2.3)$$

whose trace is simply the Laplace-Beltrami operator acting on the space spanned by the pNGBs. Notably, this depends on the geometry of the manifold on which the pNGBs live. In all of our applications we will be interested in the scenarios in which the spontaneous symmetry breaking pattern is

$$\frac{\text{SO}(N+1)}{\text{SO}(N)} \cong \mathcal{S}^N , \quad (2.4)$$

which we recall consists of the set of points a fixed distance from the origin in \mathcal{R}^{N+1} . For the sake of illustration, we focus on scenarios in which the explicit symmetry breaking follows the same pattern, preserving the $\text{SO}(N)$ subgroup. As a result, we may parameterise the N Goldstone bosons on this manifold through the unit vector living in \mathcal{R}^{N+1} as

$$\phi = f \sin \frac{\Pi}{f} \begin{pmatrix} \mathbf{n}_1 \\ \mathbf{n}_2 \\ \vdots \\ \mathbf{n}_N \\ \cot \frac{\Pi}{f} \end{pmatrix} , \quad (2.5)$$

where $\mathbf{n} \cdot \mathbf{n} = 1$. Thus, in this picture, Π/f essentially corresponds to the angle between the Goldstone boson direction and a given arbitrarily chosen axes in \mathcal{R}^{N+1} .

In these coordinates we have that the relevant mass-squared matrix is

$$\mathcal{M}_\varepsilon^2(\Pi) = \varepsilon \begin{pmatrix} \frac{\cot(\frac{\Pi}{f})}{f} V'_\varepsilon \mathbb{1}_{N-1} & 0 \\ 0 & V''_\varepsilon \end{pmatrix} . \quad (2.6)$$

where

$$V'_\varepsilon \equiv \frac{\partial V_\varepsilon}{\partial \Pi} \quad \text{and} \quad V''_\varepsilon \equiv \frac{\partial^2 V_\varepsilon}{\partial \Pi^2} . \quad (2.7)$$

Thus, considering the traces of products of this matrix which will arise in perturbative calculations, it suffices to consider the Laplace-Beltrami operator

$$\Delta_{\mathcal{S}^N} V_\varepsilon = V''_\varepsilon + (N-1) \cot \frac{\Pi}{f} \frac{V'_\varepsilon}{f} . \quad (2.8)$$

As a result, truncating the momentum integral at the UV-cutoff, the zero-temperature

effective potential at one-loop is

$$\begin{aligned}
V &= V^{(0)} + V^{\text{CW}} + V^{\text{CT}} \tag{2.9} \\
&= \varepsilon \left[V_\varepsilon + \frac{M^2}{32\pi^2} \Delta_{\mathcal{S}^N} V_\varepsilon + V_\varepsilon^{\text{CT}} \right] + \\
&\quad \varepsilon^2 \left[V_{\varepsilon^2} + \frac{1}{64\pi^2} \left\{ (V_\varepsilon'')^2 \left(\log \left(\frac{\varepsilon}{M^2} V_\varepsilon'' \right) - \frac{1}{2} \right) \right. \right. \\
&\quad \left. \left. + (N-1) \left(\frac{\cot \frac{\Pi}{f}}{f} V_\varepsilon' \right)^2 \left(\log \left(\frac{\varepsilon}{M^2} \frac{\cot \frac{\Pi}{f}}{f} V_\varepsilon' \right) - \frac{1}{2} \right) \right\} \right. \\
&\quad \left. + \frac{M^2}{32\pi^2} \Delta_{\mathcal{S}^N} V_{\varepsilon^2} + V_{\varepsilon^2}^{\text{CT}} \right] + \mathcal{O}(\varepsilon^3) + \dots
\end{aligned}$$

Here the terms denoted V^{CT} represent the counterterms required to renormalise the pNGB potential and $V^{(0)}$ is the tree-level scalar potential. Thus we see that if $\Delta_{\mathcal{S}^N} V_\varepsilon$ has a very different functional form to V_ε , the counterterm potential cannot be similar in form to V_ε , implying some level of fine-tuning between UV/threshold corrections, which must exist, and the bare potential in order to realise the form of V_ε . If, however, they are of a similar functional form then the $\mathcal{O}(\varepsilon)$ corrections will not destabilise the pNGB potential at that order. We will return to this possibility in due course.

More immediately relevant is that the $\mathcal{O}(\varepsilon^2)$ effective potential corrections may significantly modify the qualitative nature of the potential. This would signify the breakdown of the effective description of the pNGB potential. Thus we will only work with EFTs for the pNGBs in which ε is sufficiently small that the physics of the zero-temperature potential is well described at leading order in ε , hence

$$V \approx \varepsilon \left(V_\varepsilon + \frac{M^2}{32\pi^2} \Delta_{\mathcal{S}^N} V_\varepsilon + V_\varepsilon^{\text{CT}} \right) , \tag{2.10}$$

is a reasonable approximation to the pNGB potential at zero temperature. This can only be diagnosed on a case-by-case basis, and so we leave further discussion of this aspect until a specific model has been chosen.

Now moving to finite temperature and following by analogy with the Coleman-Weinberg potential, under the same set of assumptions, the full finite-temperature potential at one-loop is, to a leading approximation,

$$V(T) = V^{(0)} + V^{\text{CW}} + V^{\text{CT}} + V^{\text{T}} , \tag{2.11}$$

where [11]

$$V^{\text{T}} = \frac{T^4}{2\pi^2} \text{Tr} J_B \left(\frac{\mathcal{M}^2(\Pi)}{T^2} \right) , \tag{2.12}$$

$$= \frac{T^4}{2\pi^2} \left(J_B \left(\frac{\varepsilon V_\varepsilon''}{T^2} \right) + (N-1) J_B \left(\frac{\varepsilon \cot \left(\frac{\Pi}{f} \right) V_\varepsilon'}{f T^2} \right) \right) , \tag{2.13}$$

and the function J_B is

$$J_B(x) = \int_0^\infty dy y^2 \log \left(1 - \exp^{-\sqrt{y^2+x}} \right) . \quad (2.14)$$

Since we now have a new energy scale in the theory, T , we ought to reconsider the conditions under which one has an appropriate description of the physics. For $T \rightarrow 0$ we have that $V^T \rightarrow 0$, as expected, thus at very low temperatures we may simply use the zero-temperature effective potential already described.

At high temperatures we may also perform an expansion, in which case

$$V^T \approx -N \frac{\pi^2}{90} T^4 + \varepsilon \frac{T^2}{24} \Delta_{\mathcal{S}^N} V_\varepsilon - \frac{T}{12\pi} (\varepsilon V_\varepsilon'')^{3/2} - (N-1) \frac{T}{12\pi} \left(\varepsilon \cot \frac{\Pi}{f} \frac{V_\varepsilon'}{f} \right)^{3/2} + \dots . \quad (2.15)$$

The validity of this expansion rests on two separate aspects. The first is that the high-temperature expansion should be convergent, hence when the system lies at high enough temperatures we require that the physics is, to a good approximation, described by the second term alone, with the third remaining a subleading correction. The second aspect concerns the non-analyticity of the J_B function, and hence of the third term of eq. (2.15). This non-analyticity generates imaginary terms in the effective potential in regions where $\partial^2 V^{(0)}(\Pi)/\partial \Pi^2 < 0$. Since the effective potential is, by definition, a real scalar quantity this signals a breakdown in the effective description of the physics.

Without committing to a specific model in which one can calculate the magnitude of the various terms this is as far as we may proceed, thus we now commit to a specific class of scenarios.

3 Gegenbauer Goldstones

Experience with many physical systems, including electrostatics and thermodynamics, suggests that when one encounters the Laplacian the natural functions to work with are the eigenfunctions, satisfying an equation of the form $\Delta_{\mathcal{S}^N} V_\varepsilon(\Pi) \propto V_\varepsilon(\Pi)$. This is an eigenfunction problem and the solutions which are analytic in Π are the well-known Gegenbauer polynomials [8]

$$\Delta_{\mathcal{S}^N} G_n^{\frac{N-1}{2}}(\cos \Pi/f) = -\frac{n(n+N-1)}{f^2} G_n^{\frac{N-1}{2}}(\cos \Pi/f) , \quad (3.1)$$

where the eigenvalues and eigenfunctions are characterised by the two integers, $N \geq 1$ and $n \geq 0$. In the application to the pNGB potential, these integers are related to the explicit symmetry breaking pattern $\text{SO}(N+1) \rightarrow \text{SO}(N)$ realised by a symmetry-breaking spurion in the n -index symmetric irrep of $\text{SO}(N+1)$ [8].

Motivated by this we will thus consider a zero-temperature pNGB potential of the form

$$\begin{aligned} V(\Pi, 0) &\approx \varepsilon_n V_{\varepsilon_n} + \mathcal{O}(\varepsilon^2) \\ &\approx \varepsilon_n f^2 M^2 G_n^{\frac{N-1}{2}}(\cos \Pi/f) + \mathcal{O}(\varepsilon^2) + \dots . \end{aligned} \quad (3.2)$$

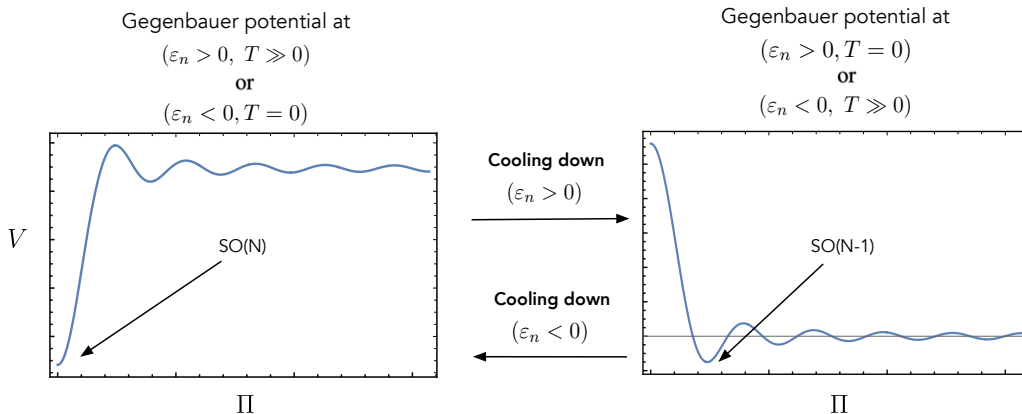


Figure 1. A cartoon picture showing the functional form of the Gegenbauer thermal effective potential given by eq. (3.7), for the temperature asymptotics $T = 0$ and $T \gg 0$, when the symmetry-breaking parameter, ε_n , is either positive or negative. The high-temperature limit terminates below the radial mode mass M , otherwise the original, approximate, symmetry is restored and the effective description of the model in terms of pNGBs is lost. Cooling down will lead to $SO(N)$ symmetry restoration or breaking depending on the sign of ε_n .

where note that from now on ε would carry the subscript n to distinguish the above choice from the general pNGB case of eq. (2.10). No summation over the index n is implied. The typical shape of the Gegenbauer potential at zero temperature ($T = 0$) is shown in the left ($\varepsilon_n < 0$) and right ($\varepsilon_n > 0$) panels of Fig. 1. Note that for positive ε_n the global minimum is at a scale $\langle \Pi \rangle \sim 5.1f/n$ [8], whereas for negative ε_n the global minimum is at the origin. Importantly, this potential is radiatively stable, since at leading order in this spurion only this term can arise irrespective of the UV physics. Since any general potential may be constructed from a linear sum of Gegenbauer polynomials the lessons learnt from studying the single polynomial case will, in generic cases, extend to more general pNGB potentials that can arise for the $SO(N+1) \rightarrow SO(N)$ case.

3.1 pNGB Potentials at Zero Temperature

With this model we may now return to our general requirement of eq. (2.10). We consider the zero-temperature potential at one-loop

$$\begin{aligned}
 V^{(1)}(\Pi, 0) \approx \varepsilon_n \left[\left(1 - \frac{n(n+(N-1))M^2}{32\pi^2 f^2} \right) V_{\varepsilon_n} + V_{\varepsilon_n}^{\text{CT}} \right] \\
 + \varepsilon_n^2 \left[V_{\varepsilon_n^2} + V_{\varepsilon_n^2}^{\text{CT}} - \frac{1}{128\pi^2} \left(\left(V_{\varepsilon_n}''(\Pi) \right)^2 + (N-1) \frac{\cot^2 \frac{\Pi}{f}}{f^2} \left(V_{\varepsilon_n}'(\Pi) \right)^2 \right) + \dots \right], \quad (3.3)
 \end{aligned}$$

where the ellipses denote the logarithmic terms. We see that at $\mathcal{O}(\varepsilon_n)$ the quadratic divergence may be absorbed into a counterterm of the same functional form as the initial potential, reflecting the radiative stability of this potential. However, we also see that, regardless of the form of the potential at $\mathcal{O}(\varepsilon_n^2)$, there are calculable terms proportional to

ε_n^2 . In order for the EFT to be valid it is necessary that these terms are subdominant to the leading one.

Since it is the point at which the second derivative of the potential is maximal in magnitude, to establish the maximal permitted value of ε_n we now focus our discussion around the origin of field space. The Gegenbauer potential and its derivatives scale there as

$$\begin{aligned} V_{\varepsilon_n}(0) &= f^2 M^2 \frac{(n+N-2)!}{n!(N-2)!} , \\ V_{\varepsilon_n}''(\Pi) \Big|_{\Pi=0} &= \cot \frac{\Pi}{f} \frac{V_{\varepsilon_n}'(\Pi)}{f} \Big|_{\Pi=0} = -M^2(N-1) \frac{(n+N-1)!}{(n-1)!N!} . \end{aligned} \quad (3.4)$$

Thus we find the condition

$$\frac{\varepsilon_n^2}{128\pi^2} N \left(V_{\varepsilon_n}''(0) \right)^2 \ll \varepsilon_n V_{\varepsilon_n}(0) , \quad (3.5)$$

which, under eq. (3.4), is reduced to

$$|\varepsilon_n| \ll 128\pi^2 \frac{f^2}{M^2} \frac{N!(n-1)!}{(n+N-1)!n(N-1)(n+N-1)} \equiv \varepsilon_{n,\max}^0 , \quad (3.6)$$

as a necessary condition for the EFT expansion to be valid at zero temperature, hence the upper-script 0 in $\varepsilon_{n,\max}$ refers to the zero-temperature case.

3.2 pNGB Potentials at Finite Temperature

After renormalization, for this class of potentials the high (enough) temperature form is approximately

$$V(\Pi, T) \approx \varepsilon_n f^2 M^2 \left(1 - \frac{n(n+N-1)T^2}{24f^2} \right) G_n^{\frac{N-1}{2}}(\cos \Pi/f) + \mathcal{O}(\varepsilon^2) + \dots \quad (3.7)$$

Thus, for temperatures satisfying

$$T^2 \gtrsim T_F^2 = \frac{24}{n(n+N-1)} f^2 , \quad (3.8)$$

where we refer to T_F as the ‘‘Flipping Temperature’’, the overall sign of the scalar potential has changed, indicating a transition in the position of the global minimum relative to the zero-temperature potential, see Fig. 1. The functional form of the scalar potential remains unchanged up to the overall factor. We must, however, determine whether we may trust the EFT expansion at this temperature by checking the magnitude of the next term in the finite-temperature expansion.

We proceed as for the zero-temperature case, but now using the thermal potential in eq. (2.15). The effective potential becomes

$$\begin{aligned} V(\Pi, T) &\approx -N \frac{\pi^2 T^4}{90} + \varepsilon_n \left[1 - \frac{n(n+N-1)T^2}{24f^2} \right] V_{\varepsilon_n}(\Pi) \\ &\quad - \frac{T (\varepsilon_n V_{\varepsilon_n}''(\Pi))^{\frac{3}{2}}}{12\pi} - (N-1) \frac{T (\cot \frac{\Pi}{f} \varepsilon_n V_{\varepsilon_n}'(\Pi))^{\frac{3}{2}}}{12\pi f^{3/2}} + \mathcal{O}(\varepsilon_n^2) . \end{aligned} \quad (3.9)$$

Focusing around the origin of the field space and noting that the second derivative of the Gegenbauer polynomial is negative there, the relevant constraint reads

$$\left| \frac{T^2}{24} \varepsilon_n \Delta_{\mathcal{S}^N} V_{\varepsilon_n}(0) \right| \gg \left| N \frac{T}{12\pi} (\varepsilon_n V_{\varepsilon_n}''(0))^{3/2} \right|. \quad (3.10)$$

This is a necessary condition for the validity of the EFT expansion at a given temperature. For $T \approx T_F$ we get

$$|\varepsilon_n| \ll 6\pi^2 \frac{f^2}{M^2} \frac{N!(n-1)!}{(n+N-1)!n(N-1)(n+N-1)} \equiv \varepsilon_{n,\max}^{T_F}. \quad (3.11)$$

This is a stronger bound than at zero temperature, since

$$\varepsilon_{n,\max}^{T_F} = \frac{3}{64} \varepsilon_{n,\max}^0. \quad (3.12)$$

The condition eq. (3.10) is necessary for validity at any temperature but not sufficient. A stronger bound is obtained for $T = T_{\text{Crit}}$, the ‘Critical Temperature’, at which the vacuum transition is initiated. In general $T_{\text{Crit}} > T_F$, with the former defined as the temperature where the potential energy of the two relevant phases becomes degenerate (or the two phases have equal free energy density)

$$V(0, T_{\text{Crit}}) = V(\langle \Pi \rangle, T_{\text{Crit}}), \quad (3.13)$$

where $\langle \Pi \rangle$ is the pNGB value at the degenerate vacuum. From Fig. 1 note that no matter which cooling-down picture we consider, the potential admits one global minimum around the field-space origin justifying our choice of $V(0, T_{\text{Crit}})$ as the free energy of one of the degenerate phases.

Using the effective potential of eq. (3.9), assuming for now $\varepsilon_n > 0$, the above equality gives

$$T_{\text{Crit}}^2 + [B_\varepsilon T_F^2] \frac{T_{\text{Crit}}}{f} - T_F^2 = 0, \quad (3.14)$$

with the solution

$$T_{\text{Crit}} = \frac{1}{2} \left[-B_\varepsilon + \sqrt{\frac{4f^2}{T_F^2} + B_\varepsilon^2} \right] \frac{T_F^2}{f}. \quad (3.15)$$

B_ε is a dimensionless parameter defined as

$$B_\varepsilon = \frac{f \Delta V_{\varepsilon,3/2}}{12\pi \Delta V_\varepsilon} \approx \frac{f}{T_F} \left\{ \frac{T_F N (\varepsilon_n V_{\varepsilon_n}''(0))^{3/2}}{12\pi \varepsilon_n V_{\varepsilon_n}(0)} \right\} - \frac{f (\varepsilon_n V_{\varepsilon_n}''(\langle \Pi \rangle))^{3/2}}{12\pi \varepsilon_n V_{\varepsilon_n}(0)} \quad (3.16)$$

where we have defined

$$\Delta V_{\varepsilon,3/2} = N (\varepsilon_n V_{\varepsilon_n}''(0))^{3/2} - (\varepsilon_n V_{\varepsilon_n}''(\langle \Pi \rangle))^{3/2}, \quad (3.17)$$

and

$$\Delta V_\varepsilon = \varepsilon_n V_{\varepsilon_n}(0) \left(1 - \frac{V_{\varepsilon_n}(\langle \Pi \rangle)}{V_{\varepsilon_n}(0)} \right) \approx \varepsilon_n V_{\varepsilon_n}(0) > 0. \quad (3.18)$$

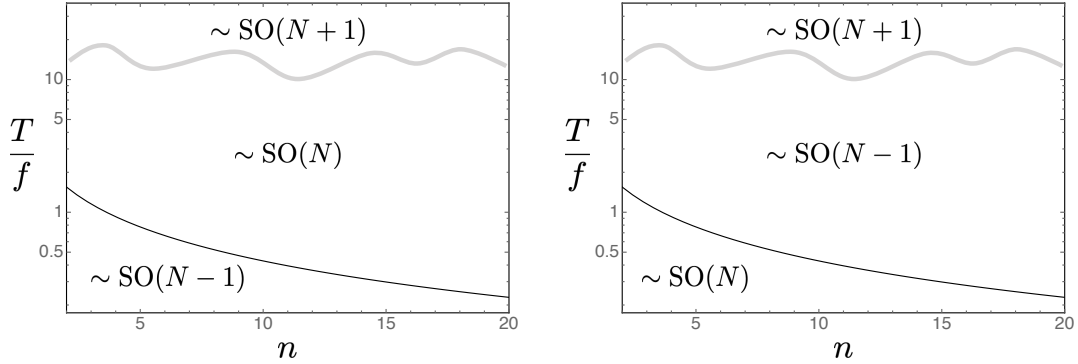


Figure 2. Schematic phase diagram for radiatively and thermally stable pNGB potentials, for $\varepsilon_n > 0$ (left) and $\varepsilon_n < 0$ (right). Throughout there is explicit breaking $SO(N+1) \rightarrow SO(N)$. At high temperatures, above the mass of the radial mode, an approximate $SO(N+1)$ is restored. For $\varepsilon_n > 0$ at lower temperatures, $SO(N+1)$ is spontaneously broken and at some lower temperature the exact $SO(N)$ is also spontaneously broken. Whereas for $\varepsilon_n < 0$ at lower temperatures, $SO(N+1)$ is spontaneously broken to $SO(N-1)$ and at some lower temperature the exact $SO(N)$ is restored.

The notion of T_{Crit} and the validity of the EFT breaks down if B_ε has large imaginary part. Note that the term included in $\{\dots\}$ above, which is purely imaginary, has been used in eq. (3.10) to derive the ε bound of eq. (3.11). However, that bound is not sufficient to make the left hand side of eq. (3.13) (and as a consequence B_ε) to a good approximation real. It is found that only for an $|\varepsilon_n|$ which is at least $\mathcal{O}(10^{-2})$ smaller than $\varepsilon_{n,\text{max}}^{T_F}$ the $\frac{f}{T_F}\{\dots\}$ term can safely be neglected from B_ε and the latter then becomes

$$B_\varepsilon \approx -\frac{f(\varepsilon_n V_\varepsilon''(\langle \Pi \rangle))^{\frac{3}{2}}}{12\pi\varepsilon_n V_{\varepsilon_n}(0)} < 0 \quad \text{and} \quad |B_\varepsilon| \ll 1, \quad (3.19)$$

and is real so we can safely evaluate the critical temperature. This stronger bound is used in this paper as the sufficient condition for the validity of the EFT in the whole relevant range of temperatures. Under that condition we obtain that $T_{\text{Crit}} \gtrsim T_F$ within a few percent. The two temperatures are sometimes identified in our qualitative discussion but kept distinct in the numerical calculations.

To summarise, we see that for this class of pNGB potentials there are hierarchies of vacuum transitions. Starting from zero temperature as the temperature is raised there will be a vacuum transition in the vicinity of the flipping temperature. Depending on the sign of the spurion this will be from zero pNGB vev to a non-vanishing one, with $\langle \Pi \rangle \propto f/n$, or vice-versa. The nature of this transition is not yet clear from this analysis, yet its existence is clear. Going to even higher temperatures, above the mass scale of the radial mode in the UV completion the standard symmetry-restoring transition occurs. These scenarios are illustrated in Fig. 2.

It is surprising and rather non-trivial that for a single spontaneous symmetry breaking scenario, with a single explicit symmetry-breaking spurion in a symmetric irrep one has a hierarchy of vacuum transitions at hierarchical scales. It remains to determine the nature of this new vacuum transition.

4 Cosmological Gegenbauer Phases

Having outlined the general phase structure of pNGB potentials it remains to determine any potential observable consequences of the additional pNGB vacuum transitions. We consider a dark sector (DS) containing pNGBs with two initial conditions after the end of inflation; thermal and supercooled, however in both cases colder than the visible sector. Given the natural origins and ubiquity of light pNGBs in quantum field theories, and given the clear evidence for the existence of dark matter, a DS scenario is well motivated and plausible. In both cases we also investigate potential stochastic GW Background signatures arising from the vacuum transitions.

4.1 Hot Dark Sector

We assume that the early universe dynamics is governed by the inflaton which, at the end of inflation, starts to oscillate about the minimum of its potential thus, due to its coupling to the Standard Model fields, the universe enters the reheating period. At the same time we consider a DS of pNGBs which is completely decoupled from (or may have an extremely small coupling to) the SM, such that it will not thermalize with the SM fields. The DS temperature, T_h , could be above or below the visible one, T_v , depending on how strongly each sector couples to the inflaton. The ratio of temperatures after reheating, $\xi_{\text{DS}} = T_h/T_v$, is heavily constrained by Big Bang Nucleosynthesis (BBN) and Cosmic Microwave Background (CMB) measurements [12, 13].

As noted, we assume $\xi_{\text{DS}} < 1$. This type of scenario has been investigated in [14, 15]. The case of $\xi_{\text{DS}} > 1$ is more delicate since it requires an out-of-equilibrium mechanism to inject entropy back into the SM before BBN, see e.g. [16]. For model-independent studies regarding the constraints on DS vacuum transition parameters see also [17, 18].¹

A general investigation of the nature of the transition is challenging and essentially beyond the reach of standard computations. However, subject to the requirement of small enough ε_n , discussed in the previous section, we may have some control in the vicinity of the flipping temperature.

To proceed let us recall that the scalar potential in the DS is a Gegenbauer polynomial. The vacuum structure of such a potential is non-trivial given that different local minima coexist for a wide range of temperatures (see Fig. 1). Analysing its thermal history in the following, a vacuum transition is expected to occur. Particularly, for $\varepsilon_n > 0$, Π obtains a non-zero vacuum expectation value and spontaneously breaks the $\text{SO}(N)$ symmetry.

Before getting into a description of the phase transition details let us present an analytic estimate for the transition strength α , assuming it takes place around $T \approx T_F$. To quantify α we use the latent heat released normalized to the radiation energy density, which can be written as

$$\alpha(T) \equiv \frac{1}{\rho_R} \left(\Delta V(\Pi, T) - \frac{T}{4} \Delta \frac{\partial V(\Pi, T)}{\partial T} \right), \quad (4.1)$$

¹Here we will not deal with the case where $\xi_{\text{DS}} = 1$, which could happen either by thermalization of the DS with the SM thermal bath or due to specific initial conditions where the inflaton couples democratically to both sectors. We escape the former by assuming the DS has a negligible interaction or never comes into contact with SM and the latter by considering a different evolution of the two sectors during reheating.

where the difference between the false and true vacuum is taken. The energy density is

$$\begin{aligned}\rho_R &= \frac{\pi^2 g_{\Pi}^* T_h^4}{30} + \frac{\pi^2 g_{\text{SM}}^*(T_v) T_v^4}{30} \\ &= \frac{\pi^2 T_h^4}{30} \left(N + \frac{g_{\text{SM}}^*(T_v)}{\xi_{\text{DS}}^4} \right)\end{aligned}\quad (4.2)$$

Since we consider a phase transition within the DS, the Hubble rate and the other relevant parameters are functions of T_h . We keep T_v as a fixed initial parameter and the number of degrees of freedom in the DS corresponds to the number of pNGBs, i.e., $g_{\Pi}^* = N$. We evaluate the radiation degrees of freedom of the SM, g_{SM}^* , from tabulated data in [19] and we keep them constant for temperatures in the vicinity of the phase transition.

Making use of the high-temperature expansion we have that the potential energy difference between false and true vacua is

$$\Delta V(\Pi, T) \approx V(0, T) - V(\langle \Pi \rangle, T) = \left[1 - \frac{T^2}{T_F^2} \right] \Delta V_{\varepsilon} - \frac{T \Delta V_{\varepsilon, 3/2}}{12\pi}, \quad (4.3)$$

while the partial derivative with respect to temperature becomes

$$\begin{aligned}\frac{T}{4} \Delta \frac{\partial V(\Pi, T)}{\partial T} &= \frac{T}{4} \left[\left. \frac{\partial V(\Pi, T)}{\partial T} \right|_{\Pi=0} - \left. \frac{\partial V(\Pi, T)}{\partial T} \right|_{\Pi=\langle \Pi \rangle} \right] \\ &\approx -\frac{1}{2} \frac{T^2}{T_F^2} \Delta V_{\varepsilon} - \frac{1}{4} \frac{T \Delta V_{\varepsilon, 3/2}}{12\pi},\end{aligned}\quad (4.4)$$

thus

$$\alpha(T) \approx \frac{\Delta V_{\varepsilon}}{\rho_R} \left(\left[1 - \frac{1}{2} \frac{T^2}{T_F^2} \right] - \frac{3}{4} \frac{T \Delta V_{\varepsilon, 3/2}}{12\pi \Delta V_{\varepsilon}} \right). \quad (4.5)$$

Focusing around T_F , which is used as a proxy for the nucleation temperature T_n since we have verified they are very close numerically, the second term in the above equation reduces to the $\{\dots\}$ term of eq. (3.16) which, as follows from the discussion above eq. (3.19), has to be very small for the validity of the EFT. Thus, the transition strength becomes

$$\alpha(T_F) \approx \frac{\Delta V_{\varepsilon}}{\rho_R} \left[1 - \frac{1}{2} \frac{T_F^2}{T_F^2} \right] = \frac{\Delta V_{\varepsilon}}{2\rho_R}. \quad (4.6)$$

By setting $\varepsilon_n = 10^{-2} \varepsilon_{n, \text{max}}^{T_F}$ we obtain

$$\alpha(T_F) \lesssim \frac{0.002}{\left(1 + \frac{g_{\text{SM}}^*(T_v)}{\xi_{\text{DS}}^4 N} \right)}. \quad (4.7)$$

The phase transition is weak because of the strong upper bound on ε_n , which also controls the magnitude of the explicit breaking of the original symmetry. This value of α corresponds to, at most, a very weakly first-order transition and suppressed gravitatonal wave spectrum.

Since the phase transition occurs at finite temperature under the presence of a non-negligible thermal plasma formed out of a system of pNGBs, the expanding bubble walls

transmit a substantial energy density and pressure to the surrounding plasma. Hence, the dominant source of GW production is the motion of the plasma itself, expressed in the form of sound waves. As described in greater detail in an app. (A), for the GW spectrum, under the assumption of small α , the peak of the spectrum is [20–23]

$$\Omega_{\text{sw}}(\text{Peak})h^2 \approx 4 \times 10^{-7} (R_* H_*)^2 (\kappa_{\text{sw}} \alpha)^{\frac{3}{2}}, \quad (4.8)$$

where κ_{sw} encodes kinetic energy normalized to vacuum energy. We evaluate the efficiency factor κ_{sw} using the numerical fits of [24]. R_* is the average bubble size at collision. As described in app. (A), we find that numerically, at the time of the transition, one has $R_* H_* \sim 10^{-6}$. Hence we expect at most to have a spectral peak of magnitude

$$\Omega_{\text{sw}}(\text{Peak})h^2 \lesssim 4 \times 10^{-23}, \quad (4.9)$$

well below the expected reach of future gravitational wave detectors.

4.2 Supercooled Dark Sector

Let us now explore the extreme possibility that our pNGB DS is supercooled, parameterized as $\xi_{\text{DS}} \approx 0$. This may occur if, for instance, the DS is very weakly coupled to the inflaton. We also discuss the role of ε_n 's sign. In the previous section we have assumed that $\varepsilon_n > 0$. However, in principle, ε_n can be either positive or negative and, as we explain in the following, the choice of sign impacts the cosmology of the DS.

It is possible that the expansion rate of the universe is initially much faster than the bubble nucleation rate in a supercooled DS.² As a consequence the DS can enter a period of supercooling, remaining in a local minimum until quantum tunneling towards another local or a global minimum takes place.

For $\varepsilon_n \gtrsim 0$ the vacuum dynamics of a supercooled DS is governed by the zero-temperature potential of eq. (3.2). Such a scenario has interesting phenomenology as the associated potential possesses various local minima and as a consequence the supercooled DS could in principle exhibit successive vacuum transitions, depicted on Fig. 3, via tunneling. For an indicative example we consider the case when the DS is initially in the minimum depicted by the purple dot in Fig. 3 with associated vev $\langle \Pi_{\text{purple}} \rangle$. We calculate the probability of tunneling towards its nearest neighbor blue dot with associated vev $\langle \Pi_{\text{blue}} \rangle$. For this transition it is clear that the barrier between the vacua is large compared to the energy difference between them, therefore the thin wall approximation [25] is a well motivated analytic approach. According to this approximation and following [15], the probability of nucleating a critical bubble via quantum tunneling is

$$\Gamma_4 = A_4 e^{-S_4} \equiv \frac{1}{R_0^4} \left(\frac{S_4}{2\pi} \right)^2 e^{-S_4} \quad (4.10)$$

where S_4 is the $O(4)$ -symmetric bounce solution and R_0 is the size of the nucleating bubble.

²Since the DS is almost decoupled from the SM it will evolve independently, so we consider that the visible sector is “frozen” to a given temperature T_v .

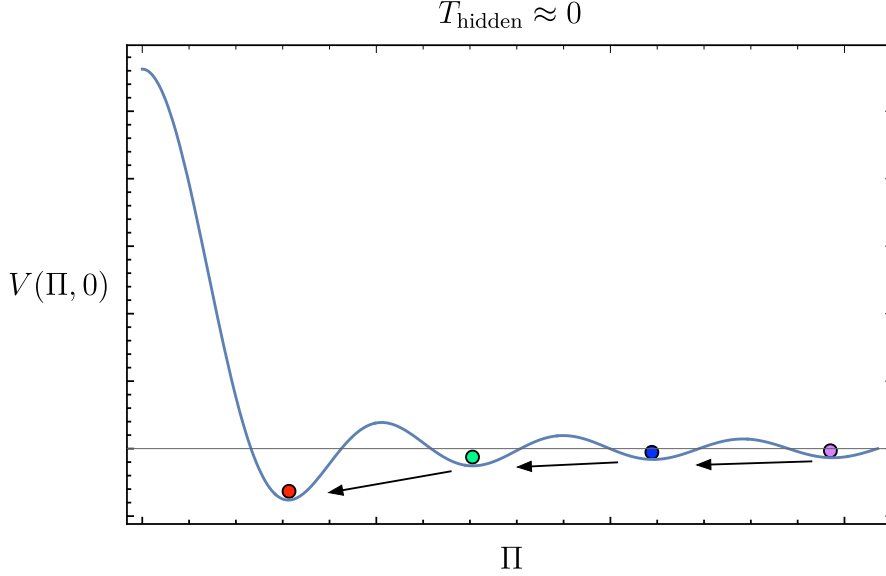


Figure 3. Successive tunneling towards the true vacuum for the benchmark scenario $n = 15, N = 4$. The colouring shows that we move from a higher $\langle \Pi \rangle$ (purple dot) down to smaller values until the DS reaches the deepest minimum (red dot).

Moreover, following the cosine-like approximation to the Gegenbauer potential provided in Eq. (2.12) of [8], and employing the triangle approximation to the cosine potential, for which an analytic expression was derived in [26], in the thin wall approximation the bounce action S_4 scales as

$$S_4 \approx \frac{32\pi^2}{3} \frac{(\Delta V_{\text{Max}}(\Pi))^2 (\Delta \Pi)^4}{(\Delta V(\Pi))^3} , \quad (4.11)$$

where $\Delta \Pi$ is the leading order change in vev between vacua, $\Delta V(\Pi)$ is the change in vacuum energy between the two vacua and $\Delta V_{\text{Max}}(\Pi)$ is the change in vacuum energy between the vacuum and the top of the barrier between them.

The resulting expression for the bounce, in the large n limit, is

$$S_4 \sim \frac{2^{3-n-N} n^2 \pi^5 \Gamma(n+N)}{3(N-1)^4 \Gamma\left(\frac{n+1}{2}\right) \Gamma\left(\frac{N}{2}\right) \Gamma\left(\frac{n+N-1}{2}\right)} \times \frac{\varepsilon_{n,\text{max}}^0}{\varepsilon_n} , \quad (4.12)$$

which ultimately scales proportional to $n!/((n/2)!)^2$, quickly becoming very large for large n . We also have that

$$R_0^4 \approx \frac{S_4}{\pi^2 \Delta V(\Pi)} \quad (4.13)$$

so substituting the above relations back to eq. (4.10) it becomes clear that for $\varepsilon_{n,\text{max}}^0/\varepsilon_n$ satisfying the criteria for a controlled EFT expansion the exponential becomes extremely small. The condition for a successful completion of the vacuum transition is

$$\Gamma_4 \gtrsim H^4 , \quad (4.14)$$

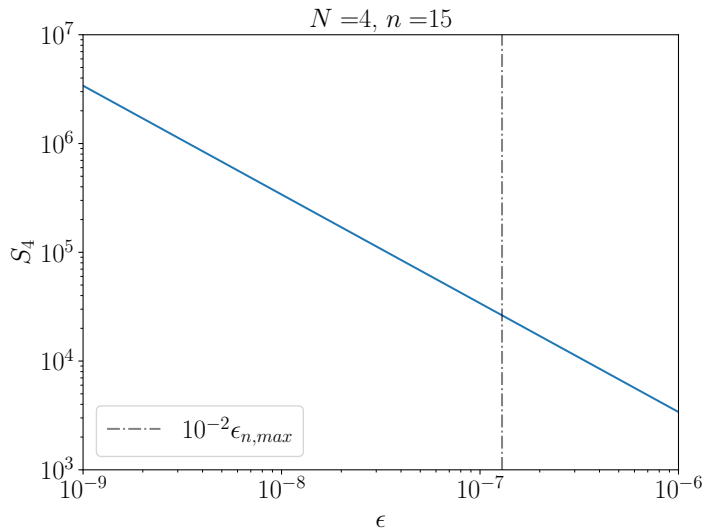


Figure 4. The bounce solution S_4 evaluated numerically as a function of ϵ for the *green dot* \rightarrow *red dot* transition as they are represented in Fig. 3.

which is difficult to fulfil. In conclusion, if the DS is for some reason localized at the *purple dot* then it will face an extremely slow decay rate, compared with the expansion of the universe, such that it will never completely tunnel to the *blue dot* in a time scale which is relevant, leading to an eternally-inflating DS.

Naturally one is led to consider the other tunneling possibilities. Naïvely for transitions closer to the true global minimum one, such as the *green to red dot* vacuum transition (see Fig. 3), one does not expect a dramatic change since the difference in vacuum energy and the height of the barrier grow in a correlated manner, however eq. (4.11) suggests that the change in vacuum energy may ultimately dominate such that faster tunnelling may be possible. In such transitions the energy difference is comparable to the barrier height, hence the thin wall approximation cannot be trusted and a numerical analysis of the bounce action is required. To this end we rely again on a modified version of CosmoTransitions [27] code. The numerical analysis of the bounce solution as a function of ϵ_n , for the benchmark scenario studied here, is shown in Fig. 4, demonstrating that only a case of a large ϵ_n , well above the upper value for an effective description of the pNGB potential, admits values of S_4 which could allow the vacuum transition to complete.

To conclude, we find that a supercooled vacuum transition in a DS with a single Gegenbauer potential and $\epsilon_n > 0$, is highly unlikely to successfully complete unless ϵ_n violates the EFT bound, in which case calculability is called into question.

PT from a flipped potential

Now consider the case with $\epsilon_n < 0$, as displayed in Fig. 5. We focus on the transition from the second minimum to the origin. Notice that this process corresponds to a symmetry-restoring phase transition since the pNGB order parameter Π has a zero vev in the true

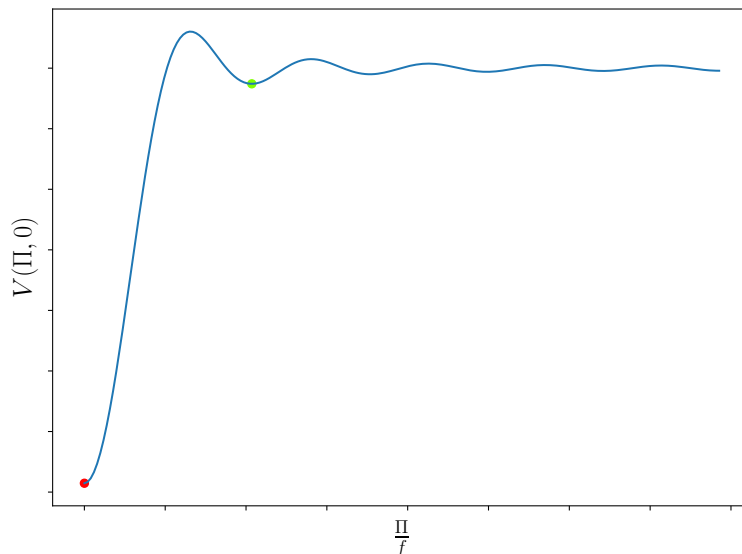


Figure 5. *Inverted tree-level Gegenbauer potential. With the transition from the green dot to the red dot considered.*

vacuum. This transition is outside the validity of the thin-wall approximation thus we compute the constant decay rate, eq. (4.10), numerically. To estimate the bubble radius at nucleation, R_0 , we use the value at which the field profile function is halfway between the two minima.

The Hubble rate is written as

$$H^2 \equiv \frac{\pi^2 g_{SM}^*(T_v) T_v^4}{90 M_{\text{Pl}}^2} + \frac{\Delta V(\Pi, 0)}{3 M_{\text{Pl}}^2}, \quad (4.15)$$

where the first term comes from the standard radiation degrees of freedom. The second term above is the vacuum contribution and we have assumed that the DS temperature remains negligibly small. For simplicity, we fix the value of $\varepsilon_n = 10^{-2} \varepsilon_{n, \text{max}}^0$ and the resonance mass scale to $M = 4\pi f$. Thus only N , n and the symmetry breaking scale f are free parameters.

The tunnelling rate Γ_4 is independent of the visible sector temperature and instead all the temperature dependence is encoded in eq. (4.15). We also find that the polynomial order n has a negligible impact on the decay rate. Once one fixes N , n and f , one has that $\Gamma_4/H^4 \propto 1/T_v^8$ for large T_v . As the temperature drops the vacuum contribution starts dominating the Hubble rate and $\Gamma_4/H^4 \approx \text{const}$. This behavior is displayed in Fig. 6 for $N = 10$ and $n = 20$ and several values of symmetry breaking scale f . One can observe from this figure that the nucleation temperature is directly proportional to the compositeness scale f , as expected on dimensional grounds. Notice that if a transition is too slow to occur at $T_v = 0$ then it cannot start for any T_v . In addition, since the potential is effectively temperature-independent, the strength parameter of the phase transition is approximately

$$\alpha(T_v) \approx \frac{\Delta V(\Pi, 0)}{\rho_R}. \quad (4.16)$$

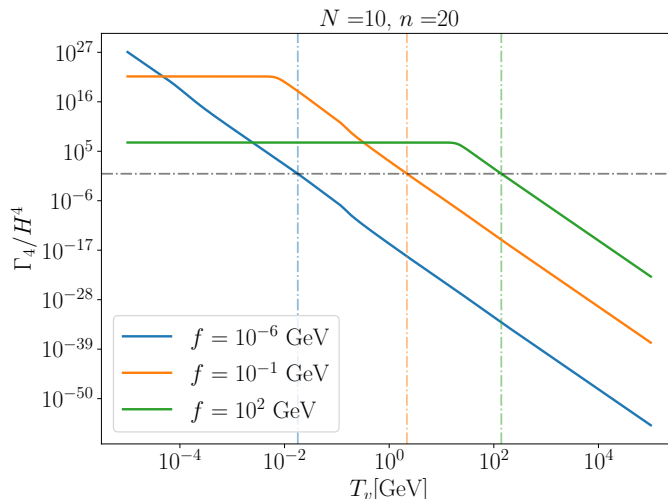


Figure 6. Ratio of nucleation rate to Hubble volume as a function of visible sector temperature for different values of the compositeness scale. The horizontal line marks the nucleation condition while the vertical lines help visualize the intersection point. At high temperatures $\Gamma_4/H^4 \propto 1/T_v^8$ while as the temperature drops the vacuum contribution begins dominating the Hubble rate and $\Gamma_4/H^4 \approx \text{const.}$

In Fig. 7 we show this transition strength (colorbar) alongside the behavior of the nucleation temperature as a function of symmetry breaking scale for two benchmark values of N . The number of pNGBs, N , significantly impacts the possible range of nucleation temperature due to the fact that, in our chosen parametrization, N affects the barrier height and thus, through the bounce action, impacts the tunneling rate exponentially. The lines terminate at the symmetry breaking scale f for which the nucleation rate matches the minimum value $\Gamma_4 \approx H^4$, as can be inferred from Fig. 6. Close to this point, the nucleation condition becomes numerically ambiguous. For smaller values of f the lines are truncated at values with extremely weak vacuum transitions. It can be observed that the strongest phase transitions are associated with the largest possible symmetry breaking scale and can attain values $\alpha \approx \mathcal{O}(1)$.

For very strong phase transitions the latent heat released accelerates the wall to relativistic velocities and the effects of the thermal plasma are suppressed. Thus the DS plasma of pNGBs exerts negligible friction on the wall and one has $v_w \approx 1$. In this case the GW signal is sourced by the collision of the walls and not by the sound waves, thus the treatment differs from sect. 4.1. To estimate the time scale of the transition we consider the bubble number density, which for a constant decay rate reads [28]³

$$\frac{1}{R_*^3} = \frac{1}{4} \left(\frac{\Gamma_4}{v_w} \right)^{3/4} \Gamma \left(\frac{1}{4} \right) \left(\frac{3}{\pi} \right)^{1/4} = \frac{1}{8\pi} \frac{\beta^3}{v_w^3}. \quad (4.17)$$

³In this expression, the gamma function $\Gamma(x)$ should not be confused with the decay rate Γ_4 .

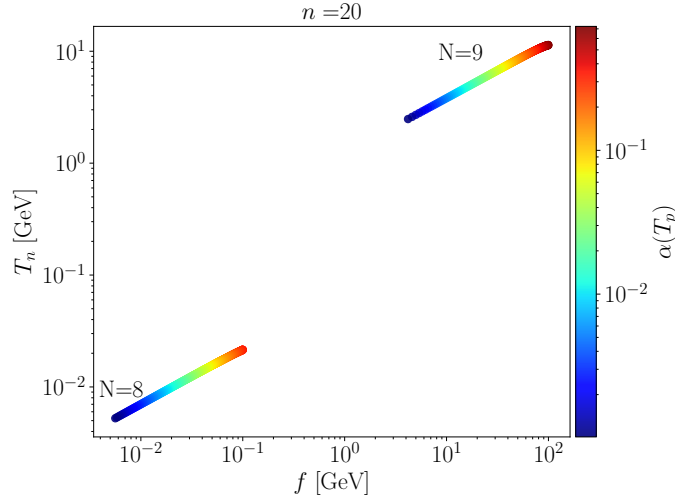


Figure 7. Nucleation temperature as a function of symmetry breaking scale f with the colorbar displaying the strength parameter α at the percolation temperature.

The GW spectrum from bubble collisions is estimated as [18]

$$\Omega_{\text{GW}}(f)h^2 = \tilde{\Omega} \times S \left(\frac{f_g}{f_{\text{col}}} \right), \quad (4.18)$$

where we write the amplitude in terms of mean bubble separation as

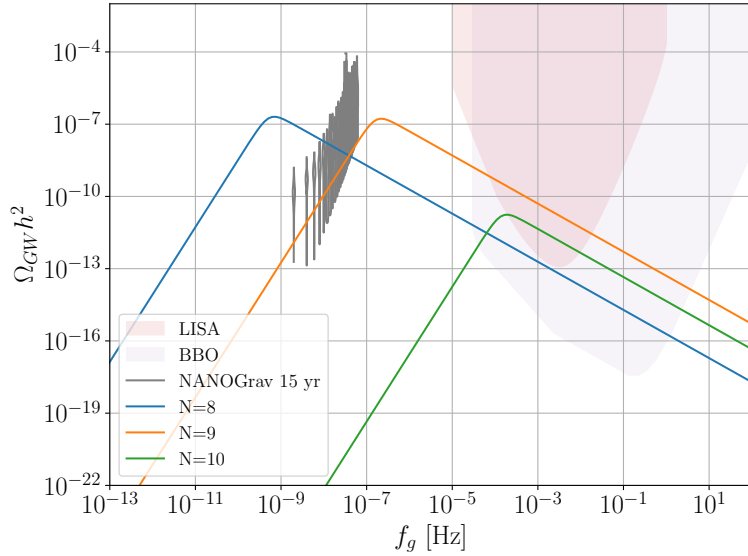


Figure 8. GW spectrum from bubble collisions for the strongest signals found. The red contours are the violin curves for the NANOGrav 15 yr data obtained from [29] using the public tool [30]. The integrated sensitivity curves for LISA and BBO were obtained using [31].

$$\tilde{\Omega} \approx 1.7 \times 10^{-5} \tilde{\Omega}_{\text{bw}} (H_{\text{min}} R_*)^2 (8\pi)^{-2/3} \left(\frac{\kappa_\phi \alpha(T_p)}{1 + \alpha(T_p)} \right)^2 \left(\frac{g_*(T_p)}{100} \right)^{-1/3}, \quad (4.19)$$

where $H_{\min}^2 = \Delta V/3M_{\text{pl}}^2$, the coefficient κ_ϕ is obtained from the detonation approximation from [24] and the spectral function is given by

$$S(x) = \frac{19x^{14/5}}{5 + 14x^{19/5}}. \quad (4.20)$$

After red-shifting the peak amplitude we have that

$$f_{\text{col}} = 1.7 \times 10^{-5} (R_* H_{\min})^{-1} (8\pi)^{1/3} \left(\frac{T_p}{100 \text{ GeV}} \right) \left(\frac{g_*(T_p)}{100} \right)^{1/6} \left(\frac{f_{\text{peak}}}{\beta} \right) \text{ Hz}, \quad (4.21)$$

with $f_{\text{peak}}/\beta \approx 0.2$, $\tilde{\Omega}_{\text{bw}} \approx 0.08$. In the expressions above we have used a slightly more precise percolation temperature, at which the probability to find a region of space-time still in the false vacuum has decreased to about $P(T_p) \sim e^{-1}$.

We show, in Fig. 8, the predicted GW spectrum from bubble collisions for three benchmark values of N where in each case we select the value of f which maximises the strength of the phase transition. We display the sensitivities of the future detectors LISA [32, 33] and BBO [34]. As we can observe from this figure, the case $N = 9$ could potentially explain the recently observed common-red spectrum from the NANOGrav 15 yr data [29] which is shown as the gray curves.

5 Summary and conclusions

The vacuum structure and dynamics of theories possessing pNGB fields in the IR is of theoretical interest and physical importance. Indeed, the vacuum structure of QCD itself is a rich subject rendered tractable by studying the vacuum structure of the pNGBs [35–38]. In this work we have explored a complementary facet of pNGB vacua which arises if explicit symmetry breaking occurs due to a spurion in a non-minimal representation. Here, again, there are metastable vacua, however they exist for different field values, as described in [8]. In this work, we have focused on the same $\text{SO}(N+1) \rightarrow \text{SO}(N)$ symmetry breaking pattern and investigated the resulting vacuum dynamics, which are found to be much richer than one might naïvely expect.

Our main result is that the ‘primary’ phase transition associated with spontaneous $\text{SO}(N+1) \rightarrow \text{SO}(N)$ breaking when the radial mode obtains a vacuum expectation value is not the end of the story. Below this scale the pNGBs will typically undergo additional vacuum transitions unless the sources of explicit symmetry breaking take the most minimal form.

These vacuum transitions may occur in two ways. Thermally, there is a second critical temperature scale, the ‘Flipping Temperature’, which scales proportional to $T_F \propto f/n$ and can thus naturally be well below the spontaneous symmetry breaking scale f . Crucially, at this temperature the functional form of the pNGB potential remains the same, to leading order in the spurion. However, the overall sign flips, such that the higher temperature minimum becomes the lower temperature maximum, and vice-versa for the higher temperature maximum. As a result, in the vicinity of the flipping temperature an additional vacuum

transition occurs. We find this is likely weakly first-order, at least for parameters consistent with a controlled EFT.

The second possibility arises non-thermally, if the pNGB sector becomes supercooled in a metastable state, which is not implausible given the existence of $\sim n$ different metastable vacua. In this case multiple vacuum transitions can occur, with the most likely being to a nearest neighbour. As the field approaches the global minimum the final vacuum transition can be strong enough to generate observable GWs.

The vacuum structure of our universe is of prime importance and interest in physics. It determines the ultimate fate of the observable universe and may carry lessons about the deep UV and quantum gravity itself [39]. Spontaneous symmetry breaking is ubiquitous in nature, for which Nambu-Goldstone bosons are the physical manifestation of the vacuum structure. Similarly, pNGBs manifest, through their vacuum structure, patterns of explicit symmetry breaking. As a result, physically relevant lessons concerning the vacuum structure and cosmological dynamics of nature may be learned by studying pNGBs, perhaps even the case in which the Higgs boson is a pNGB; a case we leave to further study.

Acknowledgements

The authors would like to thank Marek Lewicki and Andreas Mantziris for useful discussions. The research of F.K., M.M., S.P. and K.S. leading to these results has received funding from the Norwegian Financial Mechanism for years 2014-2021, grant nr DEC-2019/34/H/ST2/00707. M.M. also acknowledges support from the Polish National Science Center grant 2018/31/D/ST2/02048. K.S. is partially supported by the National Science Centre, Poland, under research grant 2017/26/E/ST2/00135.

A Hot Sector Calculations

We now detail a numerical investigation of the phase transition for a hot DS. The theory of the vacuum decay from a local false minima to the true global minima at zero and finite temperature has been studied extensively [40–44]. When the temperature is non-negligible the transition proceeds through thermal fluctuations by the nucleation of true vacuum bubbles within the space filled with false vacuum energy. The probability of decay per unit time and volume is

$$\Gamma_3(T) = \left(\frac{S_3(T)}{2\pi T} \right)^{3/2} T^4 e^{-S_3(T)/T}, \quad (\text{A.1})$$

where $S_3(T)/T$ is the finite temperature Euclidean action of our pNGB model and is less than the zero-temperature one, S_4 , around T_F .

The true vacuum bubble nucleates when the decay rate becomes comparable to the expansion rate of the universe. Namely, we define the bubble nucleation temperature by

$$\Gamma_3 \approx H^4 \Big|_{T \equiv T_n}, \quad (\text{A.2})$$

where the Hubble rate is given by

$$H^2 = \frac{\rho_R}{3M_{\text{Pl}}^2} + \frac{\Delta V(\Pi, T)}{3M_{\text{Pl}}^2}, \quad (\text{A.3})$$

which includes the contribution from the potential energy difference between false and true minima and $M_{\text{Pl}} = 2.4 \times 10^{18}$ GeV is the reduced Planck mass.

As mentioned earlier, the hidden and visible sectors have independent temperatures and cool at different rates. From eq. (4.2) above we can read off the total effective number of degrees of freedom as

$$g_* = \left(N + \frac{g_{\text{SM}}^*(T_v)}{\xi_{DS}^4} \right) . \quad (\text{A.4})$$

The time scale of the transition is given by

$$\frac{\beta}{H} \equiv T \frac{d}{dT} \left(\frac{S_3(T)}{T} \right) \Big|_{T \rightarrow T_n} . \quad (\text{A.5})$$

To compute the action we solve the equation of motion for the system, also known as the bounce solution. This can be considerably simplified by considering the parametrization of eq. (2.5) and allowing for a vev only in the Π direction such that

$$\square \Pi - \frac{\partial V(\Pi, T)}{\partial \Pi} = 0 . \quad (\text{A.6})$$

We use a modified version of the publicly available code CosmoTransitions [27] to compute the Euclidean action.

Finally, it is necessary to have an estimate for the bubble wall velocity. This requires an out-of-equilibrium computation of the deviation from equilibrium of all the particle distribution functions. While this is still a very active area of research [45–61], here we will adopt the analytic estimate of [57, 58]

$$v_w = \begin{cases} \sqrt{\frac{\Delta V}{\alpha \rho_R}} & \text{for } \sqrt{\frac{\Delta V}{\alpha \rho_R}} < v_J(\alpha) , \\ 1 & \text{for } \sqrt{\frac{\Delta V}{\alpha \rho_R}} \geq v_J(\alpha) , \end{cases} \quad (\text{A.7})$$

where α is the transition strength given in eq. (4.1) and $v_J = \frac{1}{\sqrt{3}} \frac{1 + \sqrt{3\alpha^2 + 2\alpha}}{1 + \alpha}$ the Chapman-Jouguet velocity which defines the upper limit for which hydrodynamic solutions can be found. Although this result is valid for simple extensions of the SM, in our case, we expect it to give us a realistic estimate. The reason is that we expect the friction force on the bubble wall to become significant due to the mass of the pNGBs at the metastable vacuum.

The sound wave source template reads⁴ [20–23] as a function of the frequency, f_g ,

$$\Omega_{\text{sw}}(f_g) h^2 = 4.13 \times 10^{-7} (R_* H_*) \left(1 - \frac{1}{\sqrt{1 + 2\tau_{\text{sw}} H_*}} \right) \left(\frac{\kappa_{\text{sw}} \alpha}{1 + \alpha} \right)^2 \left(\frac{100}{g_*} \right)^{\frac{1}{3}} S_{\text{sw}}(f_g) , \quad (\text{A.8})$$

where R_* is the average bubble size at collision and the spectral function is

$$S_{\text{sw}}(f_g) = \left(\frac{f_g}{f_{\text{sw}}} \right)^3 \left[\frac{4}{7} + \frac{3}{7} \left(\frac{f_g}{f_{\text{sw}}} \right)^2 \right]^{-\frac{7}{2}} , \quad (\text{A.9})$$

⁴We notice that there are several templates for the GW which derive from fits to different numerical simulations. In particular the template we use do not match those of, e.g. [18] but we nevertheless expect that our conclusion remain qualitatively the same regardless of which template is used.

g_* is given in eq. (A.4) and all the quantities of the GW spectrum are evaluated at the nucleation temperature $T_* = T_n \approx T_F$. The frequency at the peak of the spectrum is given by

$$f_{\text{sw}} = 2.6 \times 10^{-5} \text{ Hz} (R_* H_*)^{-1} \left(\frac{T_*}{100 \text{ GeV}} \right) \left(\frac{g_*}{100} \right)^{\frac{1}{6}}, \quad (\text{A.10})$$

while the duration of the sound wave source reads [22, 62–64]

$$\tau_{\text{sw}} H_* = \frac{H_* R_*}{U_f}, \quad U_f \approx \sqrt{\frac{3}{4} \frac{\alpha}{1 + \alpha} \kappa_{\text{sw}}}. \quad (\text{A.11})$$

For the mean bubble separation we use

$$H_* R_* \approx (8\pi)^{\frac{1}{3}} \left(\frac{\beta}{H} \right)^{-1}. \quad (\text{A.12})$$

For all the computations that follow in this subsection we have fixed the explicit symmetry breaking parameter to $\varepsilon_n = 10^{-2} \times \varepsilon_{n,\text{max}}^{T_F}$. For the UV scale at which we expect new resonances to appear we have fixed $M = 4\pi f$. Lastly, since the details of the dynamics of the finite temperature phase transition are to a good approximation controlled by the DS flipping temperature T_F , our only free parameters for this analysis are n , N , f , ξ_{DS} and T_v where the visible sector temperature is fixed above T_F .

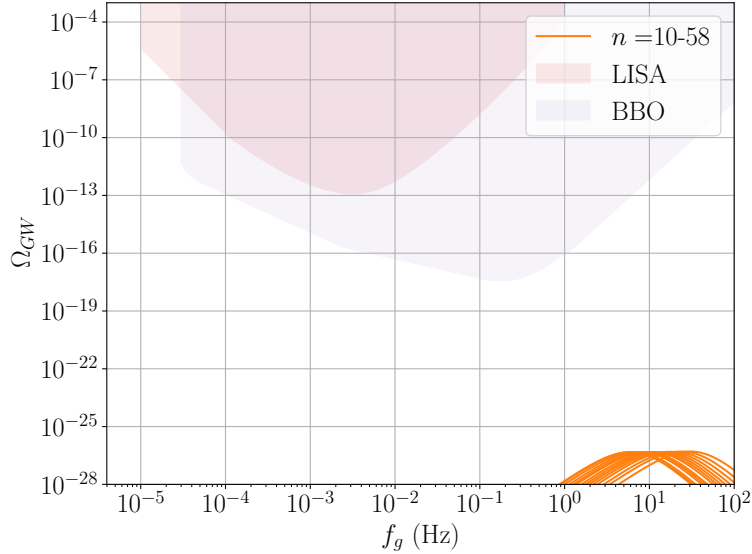


Figure 9. The GW spectrum for sound waves with $n = 10 - 58$ (orange curves). The explicit symmetry breaking parameter has been set to $\varepsilon = 10^{-2} \times \varepsilon_{n,\text{max}}^{T_F}$. The symmetry breaking scale was fixed to $f = 1 \text{ TeV}$ and the number of pNGBs to $N = 4$. The temperature of the visible sector was fixed to $T_v = 2T_F$ for each benchmark.

We present the predictions of the GW spectrum in Fig. 9 and Fig. 10 below. In Fig. 9 we display the variation of the signal as a function of the Gegenbauer polynomial order, n , while fixing $N = 4$, $f = 1 \text{ TeV}$ and $T_v = 2T_F$. We notice that the amplitude of the

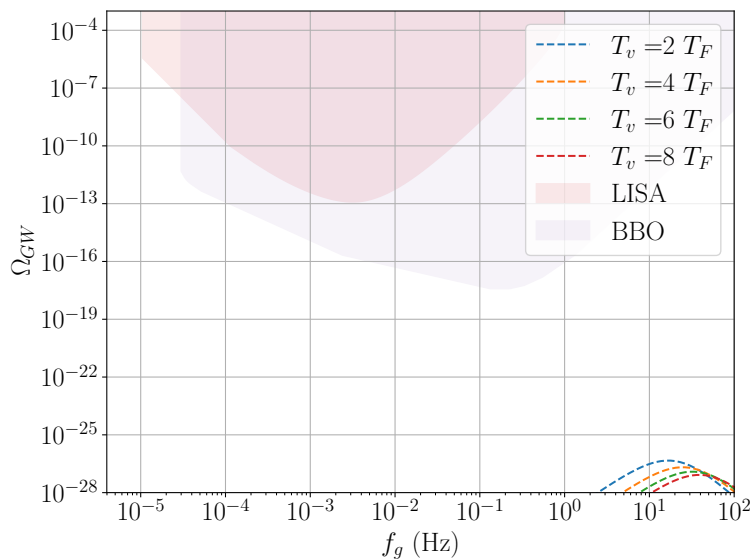


Figure 10. The GW spectrum from sound waves for $n = 20$. The explicit symmetry breaking parameter has been set to $\varepsilon_n = 10^{-2} \times \varepsilon_{n,max}^{T_F}$. The symmetry breaking scale was fixed to $f = 1$ TeV and the number of pNGBs to $N = 4$. The temperature of the visible sector was fixed as specified on the plot legends.

signal is very small compared with the expected experimental sensitivities, in particular we find $\alpha \approx 0.002$ (in agreement with our analytic prediction for the transition strength given in eq. (4.7)), $\beta/H \approx 10^6$ and $v_w \approx 0.06$. We do not observe strong dependence on the polynomial order n . Recall that $T_n \approx T_F \sim f/n$, hence the flipping temperature is numerically very close to the critical and the nucleation temperature.

In Fig. 10, we instead vary the ratio of hidden to visible temperatures by choosing different values of T_v/T_F while setting $N = 4$, $n = 20$ and $f = 1$ TeV. In this case we notice a substantial reduction in the amplitude as we increase the temperature hierarchy. This is expected as the amplitude formula eq. (A.8) is inversely proportional to the total number of degrees of freedom, in agreement with the results of [14]. Furthermore we have verified numerically that varying other parameters of the potential do not substantially change the amplitude of the signal and, irrespectively of the adopted benchmark, we obtain a strength parameter of about $\alpha \approx 0.002$ while for the inverse timescale $\beta/H \approx 10^6$ and $v_w \approx 0.06$. These numerical values are indicative of a very weak and quick transition, if not a crossover, motivating our initial choice of using T_n in the GW template formula rather than the percolation temperature.

References

- [1] Y. Nambu, *Quasiparticles and Gauge Invariance in the Theory of Superconductivity*, *Phys. Rev.* **117** (1960) 648–663.
- [2] J. Goldstone, *Field Theories with Superconductor Solutions*, *Nuovo Cim.* **19** (1961) 154–164.

- [3] S. W. Hawking, *Particle Creation by Black Holes*, *Commun. Math. Phys.* **43** (1975) 199–220. [Erratum: *Commun.Math.Phys.* 46, 206 (1976)].
- [4] Y. B. Zeldovich, *A New Type of Radioactive Decay: Gravitational Annihilation of Baryons*, *Phys. Lett. A* **59** (1976) 254.
- [5] Y. B. Zeldovich, *A Novel Type of Radioactive Decay: Gravitational Baryon Annihilation*, *Zh. Eksp. Teor. Fiz.* **72** (1977) 18–21.
- [6] T. Banks and L. J. Dixon, *Constraints on String Vacua with Space-Time Supersymmetry*, *Nucl. Phys. B* **307** (1988) 93–108.
- [7] T. Banks and N. Seiberg, *Symmetries and Strings in Field Theory and Gravity*, *Phys. Rev. D* **83** (2011) 084019, [[arXiv:1011.5120](#)].
- [8] G. Durieux, M. McCullough, and E. Salvioni, *Gegenbauer Goldstones*, *JHEP* **01** (2022) 076, [[arXiv:2110.06941](#)].
- [9] P. Binetruy and M. K. Gaillard, *Temperature Corrections in the Case of Derivative Interactions*, *Phys. Rev. D* **32** (1985) 931–937.
- [10] R. Alonso, E. E. Jenkins, and A. V. Manohar, *A Geometric Formulation of Higgs Effective Field Theory: Measuring the Curvature of Scalar Field Space*, *Phys. Lett. B* **754** (2016) 335–342, [[arXiv:1511.00724](#)].
- [11] L. Dolan and R. Jackiw, *Symmetry Behavior at Finite Temperature*, *Phys. Rev. D* **9** (1974) 3320–3341.
- [12] **Planck** Collaboration, N. Aghanim et al., *Planck 2018 results. VI. Cosmological parameters*, *Astron. Astrophys.* **641** (2020) A6, [[arXiv:1807.06209](#)]. [Erratum: *Astron.Astrophys.* 652, C4 (2021)].
- [13] T.-H. Yeh, J. Shelton, K. A. Olive, and B. D. Fields, *Probing physics beyond the standard model: limits from BBN and the CMB independently and combined*, *JCAP* **10** (2022) 046, [[arXiv:2207.13133](#)].
- [14] M. Breitbach, J. Kopp, E. Madge, T. Opferkuch, and P. Schwaller, *Dark, Cold, and Noisy: Constraining Secluded Hidden Sectors with Gravitational Waves*, *JCAP* **07** (2019) 007, [[arXiv:1811.11175](#)].
- [15] M. Fairbairn, E. Hardy, and A. Wickens, *Hearing without seeing: gravitational waves from hot and cold hidden sectors*, *JHEP* **07** (2019) 044, [[arXiv:1901.11038](#)].
- [16] F. Ertas, F. Kahlhoefer, and C. Tasillo, *Turn up the volume: listening to phase transitions in hot dark sectors*, *JCAP* **02** (2022), no. 02 014, [[arXiv:2109.06208](#)].
- [17] Y. Bai and M. Korwar, *Cosmological constraints on first-order phase transitions*, *Phys. Rev. D* **105** (May, 2022) 095015.
- [18] T. Bringmann, P. F. Depta, T. Konstandin, K. Schmidt-Hoberg, and C. Tasillo, *Does NANOGrav observe a dark sector phase transition?*, [[arXiv:2306.09411](#)].
- [19] K. Saikawa and S. Shirai, *Primordial gravitational waves, precisely: The role of thermodynamics in the Standard Model*, *JCAP* **05** (2018) 035, [[arXiv:1803.01038](#)].
- [20] M. Hindmarsh, S. J. Huber, K. Rummukainen, and D. J. Weir, *Gravitational waves from the sound of a first order phase transition*, *Phys. Rev. Lett.* **112** (2014) 041301, [[arXiv:1304.2433](#)].

- [21] M. Hindmarsh, S. J. Huber, K. Rummukainen, and D. J. Weir, *Numerical simulations of acoustically generated gravitational waves at a first order phase transition*, *Phys. Rev. D* **92** (2015), no. 12 123009, [[arXiv:1504.03291](#)].
- [22] M. Hindmarsh, S. J. Huber, K. Rummukainen, and D. J. Weir, *Shape of the acoustic gravitational wave power spectrum from a first order phase transition*, *Phys. Rev. D* **96** (2017), no. 10 103520, [[arXiv:1704.05871](#)]. [Erratum: *Phys.Rev.D* 101, 089902 (2020)].
- [23] M. B. Hindmarsh, M. Lüben, J. Lumma, and M. Pauly, *Phase transitions in the early universe*, *SciPost Phys. Lect. Notes* **24** (2021) 1, [[arXiv:2008.09136](#)].
- [24] J. R. Espinosa, T. Konstandin, J. M. No, and G. Servant, *Energy Budget of Cosmological First-order Phase Transitions*, *JCAP* **06** (2010) 028, [[arXiv:1004.4187](#)].
- [25] S. Coleman, *Fate of the false vacuum: Semiclassical theory*, *Phys. Rev. D* **15** (May, 1977) 2929–2936.
- [26] M. J. Duncan and L. G. Jensen, *Exact tunneling solutions in scalar field theory*, *Phys. Lett. B* **291** (1992) 109–114.
- [27] C. L. Wainwright, *CosmoTransitions: Computing Cosmological Phase Transition Temperatures and Bubble Profiles with Multiple Fields*, *Comput. Phys. Commun.* **183** (2012) 2006–2013, [[arXiv:1109.4189](#)].
- [28] D. Cutting, M. Hindmarsh, and D. J. Weir, *Gravitational waves from vacuum first-order phase transitions: from the envelope to the lattice*, *Phys. Rev. D* **97** (2018), no. 12 123513, [[arXiv:1802.05712](#)].
- [29] **NANOGrav** Collaboration, A. Afzal et al., *The NANOGrav 15 yr Data Set: Search for Signals from New Physics*, *Astrophys. J. Lett.* **951** (2023), no. 1 L11, [[arXiv:2306.16219](#)].
- [30] A. Rohatgi, *Webplotdigitizer: Version 4.6*, 2022.
- [31] E. Thrane and J. D. Romano, *Sensitivity curves for searches for gravitational-wave backgrounds*, *Phys. Rev. D* **88** (2013), no. 12 124032, [[arXiv:1310.5300](#)].
- [32] **LISA Cosmology Working Group** Collaboration, P. Auclair et al., *Cosmology with the Laser Interferometer Space Antenna*, [arXiv:2204.05434](#).
- [33] C. Caprini, D. G. Figueroa, R. Flauger, G. Nardini, M. Peloso, M. Pieroni, A. Ricciardone, and G. Tasinato, *Reconstructing the spectral shape of a stochastic gravitational wave background with LISA*, *JCAP* **11** (2019) 017, [[arXiv:1906.09244](#)].
- [34] V. Corbin and N. J. Cornish, *Detecting the cosmic gravitational wave background with the big bang observer*, *Class. Quant. Grav.* **23** (2006) 2435–2446, [[gr-qc/0512039](#)].
- [35] E. Witten, *Large N Chiral Dynamics*, *Annals Phys.* **128** (1980) 363.
- [36] M. Creutz, *Quark masses and chiral symmetry*, *Phys. Rev. D* **52** (1995) 2951–2959, [[hep-th/9505112](#)].
- [37] A. V. Smilga, *QCD at theta similar to pi*, *Phys. Rev. D* **59** (1999) 114021, [[hep-ph/9805214](#)].
- [38] J. March-Russell and R. Petrossian-Byrne, *QCD, Flavor, and the de Sitter Swampland*, [arXiv:2006.01144](#).
- [39] G. Obied, H. Ooguri, L. Spodyneiko, and C. Vafa, *De Sitter Space and the Swampland*, [arXiv:1806.08362](#).

- [40] S. R. Coleman, *The Fate of the False Vacuum. 1. Semiclassical Theory*, *Phys. Rev. D* **15** (1977) 2929–2936. [Erratum: *Phys.Rev.D* 16, 1248 (1977)].
- [41] C. G. Callan, Jr. and S. R. Coleman, *The Fate of the False Vacuum. 2. First Quantum Corrections*, *Phys. Rev. D* **16** (1977) 1762–1768.
- [42] S. R. Coleman and F. De Luccia, *Gravitational Effects on and of Vacuum Decay*, *Phys. Rev. D* **21** (1980) 3305.
- [43] A. D. Linde, *Fate of the False Vacuum at Finite Temperature: Theory and Applications*, *Phys. Lett. B* **100** (1981) 37–40.
- [44] A. D. Linde, *Decay of the False Vacuum at Finite Temperature*, *Nucl. Phys. B* **216** (1983) 421. [Erratum: *Nucl.Phys.B* 223, 544 (1983)].
- [45] G. D. Moore, *Electroweak bubble wall friction: Analytic results*, *JHEP* **03** (2000) 006, [[hep-ph/0001274](#)].
- [46] G. C. Dorsch, S. J. Huber, and T. Konstandin, *A sonic boom in bubble wall friction*, *JCAP* **04** (2022), no. 04 010, [[arXiv:2112.12548](#)].
- [47] A. Friedlander, I. Banta, J. M. Cline, and D. Tucker-Smith, *Wall speed and shape in singlet-assisted strong electroweak phase transitions*, *Phys. Rev. D* **103** (2021), no. 5 055020, [[arXiv:2009.14295](#)].
- [48] J. M. Cline and K. Kainulainen, *Electroweak baryogenesis at high bubble wall velocities*, *Phys. Rev. D* **101** (2020), no. 6 063525, [[arXiv:2001.00568](#)].
- [49] J. M. Cline, A. Friedlander, D.-M. He, K. Kainulainen, B. Laurent, and D. Tucker-Smith, *Baryogenesis and gravity waves from a UV-completed electroweak phase transition*, *Phys. Rev. D* **103** (2021), no. 12 123529, [[arXiv:2102.12490](#)].
- [50] B. Laurent and J. M. Cline, *Fluid equations for fast-moving electroweak bubble walls*, *Phys. Rev. D* **102** (2020), no. 6 063516, [[arXiv:2007.10935](#)].
- [51] A. Mégevand, *Friction forces on phase transition fronts*, *JCAP* **07** (2013) 045, [[arXiv:1303.4233](#)].
- [52] G. C. Dorsch, S. J. Huber, and T. Konstandin, *Bubble wall velocities in the Standard Model and beyond*, *JCAP* **12** (2018) 034, [[arXiv:1809.04907](#)].
- [53] J. Kozaczuk, *Bubble Expansion and the Viability of Singlet-Driven Electroweak Baryogenesis*, *JHEP* **10** (2015) 135, [[arXiv:1506.04741](#)].
- [54] T. Konstandin, G. Nardini, and I. Rues, *From Boltzmann equations to steady wall velocities*, *JCAP* **09** (2014) 028, [[arXiv:1407.3132](#)].
- [55] G. D. Moore and T. Prokopec, *How fast can the wall move? A Study of the electroweak phase transition dynamics*, *Phys. Rev. D* **52** (1995) 7182–7204, [[hep-ph/9506475](#)].
- [56] W.-Y. Ai, B. Garbrecht, and C. Tamarit, *Bubble wall velocities in local equilibrium*, *JCAP* **03** (2022), no. 03 015, [[arXiv:2109.13710](#)].
- [57] M. Lewicki, M. Merchand, and M. Zych, *Electroweak bubble wall expansion: gravitational waves and baryogenesis in Standard Model-like thermal plasma*, *JHEP* **02** (2022) 017, [[arXiv:2111.02393](#)].
- [58] J. Ellis, M. Lewicki, M. Merchand, J. M. No, and M. Zych, *The scalar singlet extension of the Standard Model: gravitational waves versus baryogenesis*, *JHEP* **01** (2023) 093, [[arXiv:2210.16305](#)].

- [59] M. Barroso Mancha, T. Prokopec, and B. Swiezewska, *Field-theoretic derivation of bubble-wall force*, *JHEP* **01** (2021) 070, [[arXiv:2005.10875](#)].
- [60] B.-H. Liu, L. D. McLerran, and N. Turok, *Bubble nucleation and growth at a baryon number producing electroweak phase transition*, *Phys. Rev. D* **46** (1992) 2668–2688.
- [61] B. Laurent and J. M. Cline, *First principles determination of bubble wall velocity*, *Phys. Rev. D* **106** (2022), no. 2 023501, [[arXiv:2204.13120](#)].
- [62] J. Ellis, M. Lewicki, and J. M. No, *On the Maximal Strength of a First-Order Electroweak Phase Transition and its Gravitational Wave Signal*, *JCAP* **04** (2019) 003, [[arXiv:1809.08242](#)].
- [63] J. Ellis, M. Lewicki, J. M. No, and V. Vaskonen, *Gravitational wave energy budget in strongly supercooled phase transitions*, *JCAP* **06** (2019) 024, [[arXiv:1903.09642](#)].
- [64] J. Ellis, M. Lewicki, and J. M. No, *Gravitational waves from first-order cosmological phase transitions: lifetime of the sound wave source*, *JCAP* **07** (2020) 050, [[arXiv:2003.07360](#)].